Monthly Notices
of the
ROYAL ASTRONOMICAL SOCIETY

Mon. Not. R. Astron. Soc. **414,** 2739–2750 (2011) doi:10.1111/j.1365-2966.2011.18590.x

Evidence for a circumnuclear and ionized absorber in the X-ray obscured broad-line radio galaxy 3C 445

V. Braito,[1⋆] J. N. Reeves,[2] R. M. Sambruna[3]† and J. Gofford[2]

[1]*X-Ray Astronomy Observational Group, Department of Physics and Astronomy, Leicester University, Leicester LE1 7RH*
[2]*Astrophysics Group, School of Physical and Geographical Sciences, Keele University, Keele, Staffordshire ST5 5BG*
[3]*Astrophysics Science Division, Mail Code 662, NASA Goddard Space Flight Center, Greenbelt, MD 20771, USA*

Accepted 2011 February 23. Received 2011 February 22; in original form 2010 December 16

ABSTRACT

Here we present the results of a *Suzaku* observation of the broad-line radio galaxy 3C 445. We confirm the results obtained with the previous X-ray observations which unveiled the presence of several soft X-ray emission lines and an overall X-ray emission which strongly resembles a typical type 2 Seyfert galaxy despite of the optical classification as an unobscured active galactic nucleus.

The broad-band spectrum allowed us to measure for the first time the amount of reflection ($R \sim 0.9$) which together with the relatively strong neutral Fe Kα emission line (EW $\sim$ 100 eV) strongly supports a scenario where a Compton-thick mirror is present. The primary X-ray continuum is strongly obscured by an absorber with a column density of $N_{\rm H} = 2$–3×10^{23} cm^{-2}. Two possible scenarios are proposed for the absorber: a neutral partial covering or a mildly ionized absorber with an ionization parameter log$\xi \sim 1.0$ erg cm s^{-1}. A comparison with the past and more recent X-ray observations of 3C 445 performed with *XMM–Newton* and *Chandra* is presented, which provided tentative evidence that the ionized and outflowing absorbers varied. We argue that the absorber is probably associated with an equatorial disc wind located within the parsec scale molecular torus.

Key words: galaxies: active – galaxies: individual: 3C 445 – X-rays: galaxies.

1 INTRODUCTION

X-ray observations of active galactic nucleus (AGN) are a powerful tool to understand the physical conditions of the matter in the proximity of the central supermassive black hole (SMBH) and to understand the possible connection between the accretion and outflow mechanisms. In the last decade, X-ray observations have confirmed the widely accepted Unified Model (Antonucci 1993) of AGN, which accounts for the difference between type 1 and type 2 AGNs through orientation effects. However there are still several open questions related to the geometry and physical state of the matter in the proximity of the central SMBH. In particular, a key question still to be answered is the origin of powerful relativistic jets and outflowing winds. Understanding the nature of AGN with powerful jets or disc winds is not only important in order to understand the accretion itself, but more importantly also the mechanism with which the AGN can expel the gas supply of the host galaxy quenching the growth of the SMBH and of the galaxy itself. Indeed, jets and outflows can transport a significant fraction of the mass–energy into the AGN environment, and they could represent a key to understand the AGN feedback mechanism (King & Pounds 2003; Elvis 2006; Cattaneo et al. 2009; Fabian 2010).

In the last decade, X-ray observations have successfully revealed the presence of both warm and cold gas in the central region of AGN, and have shown that ∼50 per cent of the X-ray spectra of radio-quiet AGN (RQ-AGN) present absorption and emission features due to the presence of photoionized gas, which is outflowing with typical velocities of ∼100–1000 km s^{-1} (Crenshaw, Kraemer & George 2003). On the other end, previous observations of radio-loud AGN (RL-AGN) suggested that their X-ray emission is similar to the case of RQ-AGN but with some differences. In particular, the X-ray emission appears to be harder (or flatter) and with weaker features due to reprocessing (reflection/absorption) from warm or cold gas with respect to the RQ population (Sambruna, Eracleous & Mushotzky 2002; Grandi, Malaguti & Fiocchi 2006; Ballantyne 2007). Several possible scenarios were proposed to account for these differences, among them a smaller subtending angle of the reprocessing medium as in an advection-dominated accretion flow models (Narayan & Yi 1995) or a higher ionization state of the accretion disc (Ballantyne, Fabian & Ross 2002).

Recent sensitive and broad-band observations performed with *Chandra*, *XMM–Newton* and *Suzaku* are subverting this view, indeed observations of samples of RQ- and RL-AGN have shown a large variety in the X-ray properties, with a wider range of X-ray

⋆E-mail: vb67@star.le.ac.uk
†Present address: NASA HQ, 300 E Street SW, Washington, DC, 20546.

continuum shapes where the RL sources simply populate one end of the distribution. Emission and absorption lines have been now detected also in the soft X-ray spectra of radio galaxies (Sambruna, Reeves & Braito 2007, hereafter S07; Reeves et al. 2009, 2010; Torresi et al. 2009, 2010), indicating the presence of photoionized gas in the central regions of RL-AGN analogous to RQ-AGN. Furthermore a recent analysis of the *Suzaku* observations of broad-line radio galaxies (BLRGs) has also unveiled the presence of fast outflowing gas with velocities $v \sim 0.1$–$0.3c$ and carrying substantial masses and kinetic powers similar to the radio jets (Tombesi et al. 2010).

We are currently carrying out a program of *Suzaku* observations of a sample of all the nearby ($z < 0.1$) BLRGs, for which we also have *XMM–Newton* and or *Chandra* data (3C 390.3; Sambruna et al. 2009, 3C 111; Ballo et al., in preparation; 3C 382; Sambruna et al., in preparation and 3C 445; Reeves et al. 2010). One of the goals of this project is to investigate the structure of the accretion flow and the presence of warm and cold gas in the central regions of BLRGs to better understand the jet formation. Here we focus on one of these sources 3C 445, while the X-ray properties of the sample will be presented in a forthcoming paper (Sambruna et al., in preparation).

1.1 The broad-line radio galaxy 3C 445

3C 445 is a nearby ($z = 0.057$) BLRG with a Fanaro–Riley type II morphology (Kronberg, Wielebinski & Graham 1986). The optical spectrum of 3C 445 shows the presence, in total flux, of broad emission lines [Hα full width at half-maximum (FWHM) ~ 6400 km s^{-1}; Eracleous & Halpern 1994] typical of a type 1 or unobscured AGN leading to the classification as a BLRG. The optical continuum is also highly reddened; from the large Balmer decrement (Hα/H$\beta \sim 8$), Crenshaw, Peterson & Wagner (1988) derived $E(B-V) = 1$ mag, consistent with the large Paα/Hβ ratio (5.6; Rudy & Tokunaga 1982). Assuming a standard dust-to-gas ratio, this corresponds to a column density of $N_{\rm H} \sim 5 \times 10^{21}$ cm^{-2}, which is 1 order of magnitude larger than the Galactic column density in the direction to 3C 445 ($N_{\rm H}^{\rm Gal} = 5.33 \times 10^{20}$ cm^{-2}; Murphy et al. 1996). From radio observations (Eracleous & Halpern 1998), an inclination for the jet of $i > 60^{\circ}$ is inferred, suggesting that the contribution of the jet is negligible (Doppler factor of $\delta \sim 0.2$) and also that 3C 445 is seen almost edge-on. A large viewing inclination angle for 3C 445 ($i \leq 60^{\circ}$) was also inferred by Grandi et al. (2007) with the analysis of the flux ratio of the jet components and the Very Large Array maps presented by Leahy et al. (1997).

3C 445 is a bright X-ray source ($F_{2-10\,\rm keV} \sim 7 \times 10^{-12}$ erg cm^{-2} s^{-1}), and was previously observed with all the major X-ray observatories. The analysis of an archival 15-ks *XMM–Newton* observation of 3C 445 showed a remarkable spectrum (Grandi et al. 2007; S07). The intriguing result was that, despite its optical classification as a type 1 AGN, its X-ray emission was typical of an obscured AGN in several aspects. The 2–10 keV continuum could be described by a heavily absorbed ($N_{\rm H} \sim 10^{23}$ cm^{-2}) power law with photon index $\Gamma \sim 1.4$; a narrow and unresolved Fe Kα emission line was also detected with an equivalent width of EW ~ 120 eV. Due to the limited European Photon Imaging Camera (EPIC) bandpass (0.4–10 keV), it was impossible to distinguish between a scenario with a strong reflection component (with $R \sim 2$) or a multilayer neutral partial covering absorber. However, in both the scenarios the measured $N_{\rm H}$ exceeded the column density predicted from the optical reddening. Furthermore, the soft X-ray spectrum was also reminiscent of a Compton-thin type 2 Seyfert galaxy, with several emission lines in 0.6–3 keV, due to ionized elements from O to Si.

At high energies, 3C 445 was detected with the *BeppoSAX*-PDS instrument (Grandi et al. 2006). However, due to the large field of view (FOV) of the high-energy detector onboard *BeppoSAX* and the possible contamination from a nearby cluster (A2440), this observation could provide only a weakly constrained measurement of the reflected continuum. 3C 445 is also detected with the BAT detector onboard *Swift* and is part of the 58-months catalogue[1] (Baumgartner et al. 2010).

In the soft X-ray band, the high-resolution spectra, accumulated with the *XMM–Newton*-RGS, provided the first tentative detection of the O VII and O VIII emission lines (Grandi et al. 2007). This detection suggested that the soft X-ray emission is produced in a warm gas photoionized by the AGN as observed in Compton-thin type 2 Seyfert galaxies (Bianchi, Guainazzi & Chiaberge 2006; Guainazzi & Bianchi 2007).

Recently we obtained a deep *Chandra* observation of 3C 445, which provided the evidence for both emission and absorption from photoionized gas in this obscured AGN and provided the first detailed quantitative measurement. In particular, in the *Chandra* spectrum several soft X-ray emission lines (from the He and H-like transitions of O, Ne, Mg and Si) were detected and resolved. From the ratio of forbidden to intercombination emission lines in the He-like triplets and the velocity broadening ($v_{\rm FWHM} \sim 2600$ km s^{-1}), it was inferred that the photoionized emitter has properties very similar to the broad-line region (BLR). The *Chandra* spectrum confirmed that 3C 445 is highly obscured but it was suggestive that X-ray absorber could be associated with a disc wind with an observed outflow velocity of 10 000 km s^{-1}, which is launched from a subparsec scale location.

Here we present the analysis and results from our 140 ks *Suzaku* observation of 3C 445, while the results on the high-resolution soft X-ray spectra obtained with our deep (200 ks) *Chandra* low-energy transmission grating (LETG) observation are discussed in a companion paper (Reeves et al. 2010). The *Swift*-BAT spectrum [S/N = 16.2; $F(14-195$ keV$) = 4.2 \pm 0.5 \times 10^{-11}$ erg cm^{-2} s^{-1}] is used in this paper and fitted jointly with the *Suzaku* data. We took advantage of the *Chandra* results, while modelling the *Suzaku* data (Sections 3.2 and 3.4), and we present a comparison between the two data sets, which provided tentative evidence that the X-ray absorbers varied (Sections 3.4 and 4).

The paper is structured as follows. The observation and data reduction are summarized in Section 2. In Section 3 we present the modelling of the broad-band spectrum, aimed to assess the nature of the X-ray absorber, the amount of reflection and the Fe K emission-line properties. Discussion and conclusions follow in Sections 4 and 5. Throughout this paper, a concordance cosmology with $H_0 = 71$ km s^{-1} Mpc^{-1}, $\Omega_{\Lambda} = 0.73$ and $\Omega_{\rm m} = 0.27$ (Spergel et al. 2003) is adopted.

2 OBSERVATIONS AND DATA REDUCTION

On 2007 May 25, *Suzaku* (Mitsuda et al. 2007) observed 3C 445 for a total exposure time of about 140 ks (over a total duration of $\sim$270 ks); a summary of observations is shown in Table 1. *Suzaku* carries on board four sets of X-ray mirrors, with an X-ray CCD (X-Ray Imaging Spectrometer, XIS; three front illuminated, FI,[2] and one back illuminated, BI) at their focal plane, and a non-imaging hard X-ray detector (HXD). All together the XIS and the HXD-PIN

[1] heasarc.gsfc.nasa.gov/docs/swift/results/bs58mon/

[2] At the time of this observation only XIS0 and XIS3 were still operating.

Table 1. Summary of the observations used: observatory, epoch, instrument, total and net exposure time. For *Suzaku* the total exposure time is not the elapsed time of the observation and it already includes the standard screening for the passage above the SAA anomaly. The net exposure times are after the screening of the cleaned event files.

Mission	Date	Instrument	$T_{(\mathrm{tot})}$ (ks)	$T_{(\mathrm{net})}$ (ks)
Suzaku	2007-5-25	XIS-FI	139.8	108
Suzaku	2007-5-25	XIS 1	139.8	108
Suzaku	2007-5-25	HXD-PIN	139.8	109.5
Chandra	2009-09-25	ACIS-S LETG	–	43.950
Chandra	2009-09-29	ACIS-S LETG	–	73.720
Chandra	2009-10-02	ACIS-S LETG	–	83.440

cover the 0.5–10 keV and 12–70 keV bands, respectively. Data from the XIS (Koyama et al. 2007) and HXD-PIN (Takahashi et al. 2007) were processed using v2.1.6.14 of the *Suzaku* pipeline applying the standard screening.[3]

2.1 The *Suzaku*-XIS analysis

The XIS data were selected in 3 × 3 and 5 × 5 editmodes using only good events with grades 0, 2, 3, 4 and 6, and filtering the hot and flickering pixels with the script SISCLEAN. The net exposure times are 108 ks for each of the XIS. The XIS source spectra were extracted from a circular region of 2.4 arcmin radius centred on the source, while background spectra were extracted from two circular regions of 2.4 arcmin radius offset from the source and the calibration sources. The XIS response (rmfs) and ancillary response (arfs) files were produced, using the latest calibration files available, with the FTOOLS tasks XISRMFGEN and XISSIMARFGEN respectively. The spectra from the two FI CDDs (XIS 0 and XIS 3) were combined to create a single source spectrum (hereafter XIS-FI), while the BI (the XIS1) spectrum was kept separate and fitted simultaneously. The net 0.5–10 keV count rates are (0.154 ± 0.001) count s^{-1}, (0.158 ± 0.001) count s^{-1}, (0.142 ± 0.001) count s^{-1} for the XIS0, XIS3 and XIS1 respectively with a net exposure of 108 ks for each XIS. Data were included from 0.4–10 keV for the XIS-FI and 0.4–8 keV for the XIS1 chip; the difference on the upper boundary for the XIS1 spectra is because this CCD is optimized for the soft X-ray band. The background rates in these energy ranges correspond to only 4.5 and 8.1 per cent of the net source counts for the XIS-FI and XIS1, respectively. The net XIS source spectra were then binned to a minimum of 100 count per bin and χ^2 statistics have been used.

2.2 The *Suzaku* HXD-PIN analysis

For the HXD-PIN data reduction and analysis, we followed the latest *Suzaku* data reduction guide (the ABC guide Version 2)[4], and used the rev2 data, which include all four cluster units. The HXD-PIN instrument team provides the background (known as the 'tuned' background) event file, which accounts for the instrumental non-X-ray background (Kokubun et al. 2007). The systematic uncertainty of this 'tuned' background model is believed to be ±1.3 per cent (at the 1σ level for a net 20-ks exposure).

We extracted the source and background spectra using the same common good time interval, and corrected the source spectrum for the detector dead time. The net exposure time after the screening was 109.5 ks. We then simulated a spectrum for the cosmic X-ray background counts (Boldt 1987; Gruber et al. 1999) and added it to the instrumental one.

3C 445 is detected up to 70 keV at a level of 12.9 per cent above the background corresponding to a signal-to noise ratio (S/N) ∼ 30. The net count rate in the 15–70 keV band is 0.052 ± 0.002 count s^{-1} (∼5700 net counts). For the spectral analysis, the source spectrum of 3C 445 was rebinned in order to have a S/N of 5 in each energy bin. The HXD-PIN spectrum can be fitted with a single power law ($\Gamma = 2.0 \pm 0.3$); this provides a first estimate of the 15–70 keV flux of about $\sim 3.1 \times 10^{-11}$ erg cm^{-2} s^{-1}. The extrapolated flux in the *Swift* band (14–195 keV) is $\sim 5 \times 10^{-11}$ erg cm^{-2} s^{-1} and it is comparable to the flux reported in the BAT 58-months catalogue (Baumgartner et al. 2010).

2.3 The *Swift*-BAT observation

The BAT spectrum was obtained from the 58-months survey archive, which provides both the spectrum and the long-term online BAT light curve; the data reduction procedure of the eight-channel spectrum is described in Tueller et al. (2010) and Baumgartner et al. (2010). For the analysis we used the latest calibration response file (the diagonal matrix: diagonal.rsp) provided with the spectrum, and we also inspected the light curve that shows no strong variability. The net count rate in the 14–195 keV band is $(4.2 \pm 0.3) \times 10^{-4}$ count s^{-1}.

2.4 The *Chandra* observation

Recently, 3C 445 was observed with the *Chandra* ACIS-S for 200 ks. The observation was performed on 2009 September with the LETG (Brinkman et al. 2000) in the focal plane. In this paper we concentrate on the *Suzaku* results, while the *Chandra* data reduction, analysis and results are described in a companion paper (Reeves et al. 2010). Thanks to the high sensitivity and spectral resolution the LETG data allowed us to resolve the soft X-ray emission lines, determining the gas density and location. Since 3C 445 is not highly variable either in flux and spectral shape, we were able to take the advantage of the *Chandra* results, while modelling the *Suzaku* data and vice versa.

3 SPECTRAL ANALYSIS

All the models have been fit to the data using standard software packages (XSPEC ver. 11.3). In the following, unless otherwise stated, fit parameters are quoted in the rest frame of the source and errors are at the 90 per cent confidence level for one interesting parameter ($\Delta\chi^2 = 2.71$).

3.1 The broad-band continuum

Previous X-ray studies of 3C 445 revealed that its X-ray spectrum is complex and cannot be modelled with a single power-law component. This is confirmed by our *Suzaku* observation, where the XIS curved continuum is highly indicative of the presence of strong absorption. A fit to the 0.4–10 keV XIS data with a single redshifted power-law model, modified by Galactic ($N_{\mathrm{H}} = 5.33 \times 10^{20}$ cm^{-2};

[3] The screening filters all events within the South Atlantic Anomaly (SAA) as well as with an Earth elevation angle (ELV) <5° and Earth day-time elevation angles (DYE_ELV) less than 20°. Furthermore also data within 256 s of the SAA were excluded from the XIS and within 500 s of the SAA for the HXD. Cut-off rigidity criteria of >8 GV for the HXD data and >6 GV for the XIS were used.

[4] http://heasarc.gsfc.nasa.gov/docs/suzaku/analysis/abc/

Dickey & Lockman 1990) and intrinsic (in the rest-frame of 3C 445) absorption, yields a poor fit (χ^2/d.o.f. = 3865.2/388) with a hard photon index ($\Gamma \sim -0.27$) and leaves strong residuals at low and high energies.

We then added to this model a soft power-law component absorbed only by the Galactic column, which represents the primary X-ray emission scattered into our line of sight. The photon indices of these two power-law components were constrained to be the same. This model is still a poor description of the X-ray emission from 3C 445 (χ^2/d.o.f. = 885.3/387) and as already noted with the *XMM–Newton* observation (S07) it fails to reproduce the overall curvature, which suggests that a more complex absorber is required. Furthermore, it leaves strong residuals both at the Fe Kα line energy range and in the soft X-ray band and the photon index is found to be hard ($\Gamma \sim 1.3$) with respect to the typical values of RL-AGN (Sambruna, Eracleous & Mushotzky 1999; Reeves & Turner 2000).

We then tested a model for the continuum similar to the best fit found for the *XMM–Newton* data, without including any reflection, and we ignored the 5–7.5 keV band, where the Fe Kα emission complex is expected. The absorber is now modelled with a dual absorber; one fully covering the primary X-ray emission and one only partially covering it. A scattered component, modelled with a second power-law with the same photon index of the primary one is still included. This is now a better representation of the X-ray continuum and the photon index is now steeper ($\Gamma = 1.70 \pm 0.11$). The column densities of the absorbers are found to be $N_{\rm H1} = (1.1 \pm 0.2) \times 10^{23}$ cm^{-2} and $N_{\rm H2} = (3.3 \pm 0.6) \times 10^{23}$ cm^{-2}, for the fully and partial covering absorber, respectively; the covering fraction of the latter absorber is $f_{\rm cov} = 0.79^{+0.06}_{-0.08}$, while the scattering fraction is found to be $f_{\rm scatt} \sim 0.03$.

This continuum model is still too simple with respect to the broad-band X-ray emission, indeed its extrapolation underpredicts the counts collected above 10 keV (see Fig. 1). Furthermore, as seen with *XMM–Newton* this model leaves strong line-like residuals at the energy of the Fe Kα emission line. These residuals suggest the presence of a strong narrow core at the expected energy of the Fe Kα line (6.4 keV) and a possible weak component redwards of the narrow core at $E \sim 6$ keV (observed frame), which could

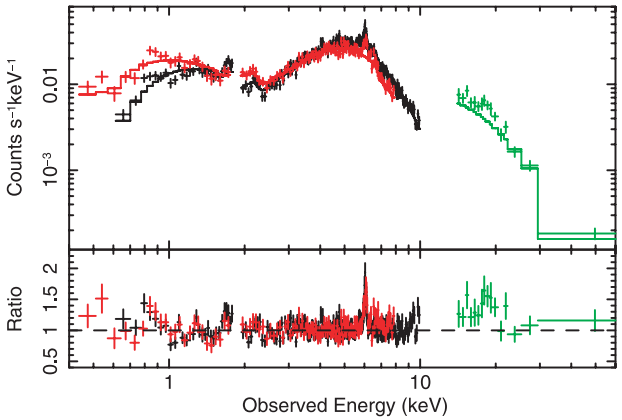

Figure 1. *Suzaku* 0.4–60 keV spectra (in the electronic version: XIS-FI, black; XIS1, red; HXD-PIN green) of 3C 445; data have been rebinned for plotting purposes. The upper panel shows the data and the dual absorber model ($\Gamma \sim 1.7$; $N_{\rm H1} \sim 10^{23}$ cm^{-2}; $N_{\rm H2} \sim 3.3 \times 10^{23}$ cm^{-2}) fitted over the 0.4–5 and 7.5–10 keV band. The lower panel shows the data/model ratio to this model. Clear residuals are visible at the iron K-shell energy band and in the HXD-PIN energy range. The excess of counts in the HXD-PIN spectrum compared to the XIS, is probably due to the Compton reflection hump.

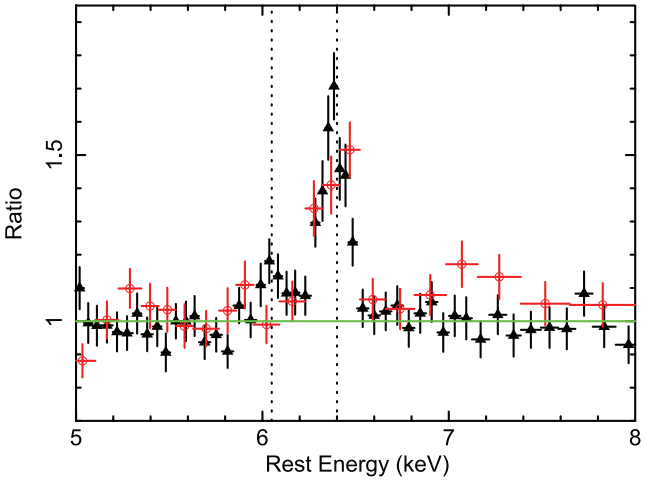

Figure 2. Data/model ratio between the XIS data (XIS-FI, black triangles in the electronic version; XIS-BI red open circles in the electronic version) and the dual absorber model showing the iron line profile. The data clearly show (indicated by the two vertical lines) a narrow core at 6.4 keV (rest frame), and a weak narrow emission feature at ∼6.1 keV (rest frame).

be identified with the Compton shoulder (see Fig. 2). Both these features and the hard excess seen in the spectrum above 10 keV suggest the presence of a strong reflection component. The presence of this latter component was already suggested with the previous *BeppoSAX* observation (Dadina 2007; Grandi et al. 2006), however taking into account the possible contamination from a nearby cluster of galaxies (A2440; $z = 0.094$) it was not possible to derive strong constraints on it.

In order to obtain a better representation of the X-ray continuum, we then fitted simultaneously the *Suzaku* XIS (0.4–10 keV) and HXD-PIN data (15–65 keV) and the *Swift*-BAT spectra. We set the cross-normalization factor between the HXD and the XIS-FI spectra to 1.16, as recommended for XIS nominal observations processed after 2008 July[5] and allowed the cross-normalization of the *Swift*-BAT data to vary, since the two observations are not simultaneous.

We included in the model the Fe Kα line and a Compton reflection component. At this stage this component was modelled with the PEXRAV model in XSPEC (Magdziarz & Zdziarski 1995), with the abundances set to solar values and the inclination angle i to 60°. We note that the cluster A2440, which was thought to contaminate the X-ray emission detected with the *BeppoSAX*-PDS instrument lies at the edge of the FOV of the HXD-PIN and thus the contamination from it should be minimal. The cross-normalization with the *Swift* data is consistent with one as indicated by the similar HXD and BAT fluxes ($C \sim 0.8$), furthermore the slope of the *Swift*-BAT spectrum is consistent with the HXD-PIN data, with no evidence of a high-energy cut-off. The similarity in flux and shape confirms that the *Suzaku* HXD-PIN spectrum is dominated by the emission of 3C 445 with no or minimal contamination from the nearby cluster. It is worth noting that since the *Swift*-BAT data allow us to extend the analysis only up to 150 keV, we cannot discriminate if the lack of any roll over is real or simply due to the still-limited bandpass and the complex curvature of the spectrum. Indeed upon leaving the

[5] http://www.astro.isas.jaxa.jp/suzaku/doc/suzakumemo/suzakumemo-2007-11.pdf;
http://www.astro.isas.jaxa.jp/suzaku/doc/suzakumemo/suzakumemo-2008-06.pdf

high-energy cut-off free to vary, we can set only a lower limit ($E > 60$ keV).

The amount of reflection, defined by the subtending solid angle of the reflector $R = \Omega/2\pi$ is found to be $R \sim 1.1 \pm 0.4$, while the parameters of the absorbers are consistent with the values obtained with the previous model ($N_{\rm H1} = 1.1^{+0.1}_{-0.1} \times 10^{23}$ cm^{-2}and $N_{\rm H2} = 3.2^{+0.4}_{-0.4} \times 10^{23}$ cm^{-2}, $f_{\rm cov} = 0.74^{+0.02}_{-0.02}$ and χ^2/d.o.f. = 496.7/408). The photon index is now $\Gamma = 1.78^{+0.08}_{-0.07}$. The Fe K$\alpha$ emission line is centred at $E = 6.384 \pm 0.012$ keV, it has an EW = 105 ± 15 eV with respect to the observed continuum and it is has a measured width of $\sigma = 37 \pm 34$ eV. We note that the inclusion of the reflection component is not only statistically required ($\Delta\chi^2 = 23$ for 1 d.o.f. or χ^2/d.o.f. = 520.1/409), but also its strength is consistent with the observed EW of the Fe Kα emission line.

This model gives a 2–10 keV observed flux of $\sim 7 \times 10^{-12}$ erg cm^{-2} s^{-1} and a intrinsic (corrected for absorption) luminosity of $\sim 1.2 \times 10^{44}$ erg s^{-1}, which is similar to the value measured with *XMM–Newton* and *ASCA*.

This model now provides a better phenomenological description of 3C 445's X-ray continuum, however statistically the fit is still poor (χ^2/d.o.f. = 496.7/408), with some residuals in the 2–10 keV band, suggesting that this model is still too approximate for the broad-band emission of 3C 445. Several line-like residuals are present at $E < 2$ keV, in agreement with the previous detection from *ASCA* and *XMM–Newton* (Sambruna et al. 1999, 2007; Grandi et al. 2007). Finally we note that without the inclusion of the *Swift*-BAT, the overall statistics (χ^2/d.o.f. = 491.7/401) and parameters, derived with this simple and phenomenological model, are similar ($\Gamma = 1.79^{+0.09}_{-0.08}$ and $R \sim 1.2 \pm 0.5$). The reflection component is also statistically required with the *Suzaku* data alone ($\Delta\chi^2 = 21$ for 1 d.o.f. or χ^2/d.o.f. = 513/402). A more detailed description of the modelling of the Fe Kα emission line and of the overall hard X-ray spectral curvature is provided in Sections 3.3 and 3.4; nevertheless we note that this modelling does not strongly affect the results of the soft X-ray emission, which are presented in the following section.

3.2 The soft X-ray spectrum

In order to model the soft X-ray emission, we allow the photon index of the soft component to vary. The photon index of the scattered component is now found to be slightly steeper, $\Gamma = 2.15 \pm 0.25$, and even at the CCD resolution of the XIS instrument several lines from O, Ne, Mg and Si are clearly detected (see Fig. 3; black and red data points). Taking into account the lower count statistics of the soft X-ray spectrum, we decided to use a finer binning for the XIS data adopting a minimum of 50 count per bin. The fit statistic of the continuum model is now χ^2/d.o.f. = 746.4/676. We first added to the continuum model several narrow ($\sigma = 10$ eV) Gaussian lines, allowing also all the continuum parameters to vary; overall, upon including six lines the fit statistic improves and it is now χ^2/d.o.f. = 662.8/676 ($\Delta\chi^2 = -83$ for 12 d.o.f.). We note that the Γ of the soft power law is now similar to the primary power-law component, we thus constrained the two photon indices to be the same.

In Table 2, we list all the detected lines with their properties, statistics and possible identification, which point towards emission from lighter elements in particular $2 \rightarrow 1$ transition of H- and He-like O, Mg and Si. Though some of the soft X-ray emission lines are not detected with high statistical significance (e.g. for Mg XI, we have $\Delta\chi^2 = 5.2$), their detection and interpretation are in agreement with the results obtained with the deep *Chandra* LETG observation (Reeves et al. 2010). The *Chandra* spectrum confirms the identification of the feature detected at $\sim$0.88 keV with O VIII radiative recombination continuum (RRC). This feature, along with the O VII RRC at $E \sim 0.74$ keV, is resolved by the *Chandra* LETG and has measured widths which imply that the emitting gas is photoionized rather than collisionally ionized.

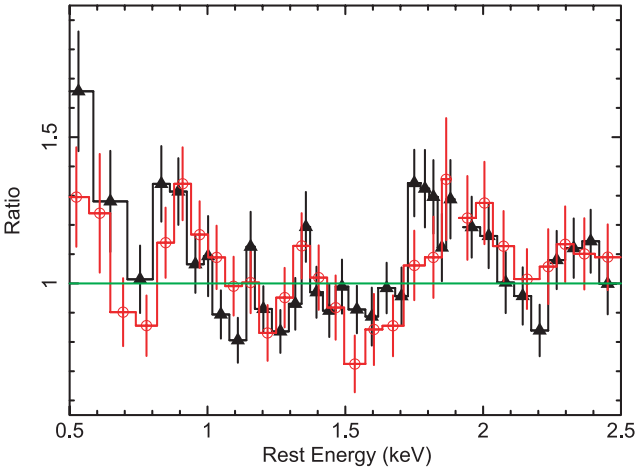

Figure 3. Zoom on the 0.5–2.5 keV range of the data/model ratio to a power-law component ($\Gamma \sim 1.7$; XIS-FI, black triangles in the electronic version; XIS-BI open red circles in the electronic version). Several emission lines are clearly present in the residuals.

Since with the *Suzaku* XIS CCD resolution we cannot resolve the line triplets and we cannot establish with high accuracy the identification of some of the lines, and taking into account that 3C 445 is not highly variable, we adopted for the soft X-ray emission the best-fitting model obtained with the *Chandra* LETG data. This model includes two grids of photoionized emission models (with $\log \xi_1 \sim 1.82$ erg cm s^{-1} and $\log \xi_2 \sim 3.0$ erg cm s^{-1}) generated by XSTAR (Kallman et al. 2004), which assumes a $\Gamma \sim 2$ illuminating continuum and a turbulence velocity of $\sigma_{\rm v} = 100$ km s^{-1} and a column density for the emitter of $N_{\rm H} = 10^{22}$ cm^{-2}. We note that the column density of the emitter cannot be directly measured from the spectrum because it is degenerate with its covering factor and thus the normalization of this component. We thus kept the value fixed to the one adopted with the *Chandra* LETG analysis. We applied this best-fitting model to the XIS soft spectrum, keeping the abundances fixed to the values measured with the LETG spectrum and allowing only the normalizations and the photon index to vary. This model is now a good description of the soft spectrum (χ^2/d.o.f. = 696.6/674) and no strong residuals are present below 3 keV. As a final test, we allowed the ionization parameter of the two emitters to vary and found a good agreement between the *Suzaku* and *Chandra* best fits ($\log \xi_1 = 1.95^{+0.14}_{-0.08}$ erg cm s^{-1} and $\log \xi_2 = 3.17^{+0.21}_{-0.23}$ erg cm s^{-1}). We note that the presence of the higher ionization emitter is not statistically required ($\Delta\chi^2 = 3$), and a good fit is found with a single zone with $\log \xi = 1.97^{+0.24}_{-0.12}$ erg cm s^{-1}. We note also that there is still a line-like residual at $\sim$2.3 keV, which cannot be modelled with these two components. We thus included in the model an additional Gaussian line, the line is found to be $E = 2.33 \pm 0.05$ keV and could be associated with S Kα. Finally, we note that both the ionization parameters and the fluxes of the ionized emitters measured with *Suzaku* are consistent with the one measured with the *Chandra* LETG data.

The extraction region of the *Suzaku* XIS spectra includes the narrow-line quasi-stellar object (QSO; 1WGA J2223.7-0206), which was first detected by *ROSAT* and which is located at about 1.3 arcmin from the 3C 445. Its X-ray spectrum obtained with

Table 2. Summary of the soft-X-ray emission lines. The energies of the lines are quoted in the rest frame. Fluxes and possible identifications are reported in column 2 and 3. For the emission feature detected at ∼0.88 keV, the alternative identifications are reported in brackets. The EW are reported in column 4 and they are calculated against the total observed continuum at their respective energies. In column 5 the improvement of fit is shown; the value for the model with no lines is χ^2/d.o.f. = 746.4/676. In column 6 we report the theoretical value for the transitions. The Γ of the soft power law is tied to the hard power-law component. We note that some of the soft X-ray emission lines are not detected with high statistical significance (e.g. for Ne X Lyα and Mg XI Heα we have $\Delta\chi^2 = 7.7$ and $\Delta\chi^2 = 5.2$, respectively).

Energy (keV) (1)	Flux (10^{-6} ph cm^{-2} s^{-1}) (2)	ID (eV) (3)	EW (eV) (4)	$\Delta\chi^2$ (5)	$E_{\rm Lab}$ (keV) (6)
$0.54^{+0.03}_{-0.02}$	$15.92^{+0.72}_{-0.70}$	O VII Heα	$47.6^{+22.3}_{-20.6}$	10.85	0.561(f); 0.569 (i); 0.574(r)
$0.88^{+0.02}_{-0.02}$	$7.37^{+1.98}_{-2.22}$	O VIII RRC (Fe XVIII–XIX)	$51.0^{+13.8}_{-14.5}$	30.0	>0.873 0.853–0.926
$0.99^{+0.01}_{-0.03}$	$2.85^{+1.45}_{-1.62}$	Ne X Lyα	$24.0^{+12.2}_{-13.6}$	7.7	1.022
$1.36^{+0.03}_{-0.03}$	$1.40^{+0.78}_{-1.14}$	Mg XI Heα	$19.5^{+11.0}_{-15.8}$	5.2	1.331(f); 1.343(i); 1.352 (r)
$1.80^{+0.03}_{-0.03}$	$2.89^{+1.31}_{-0.46}$	Si XIII Heα	$59.9^{+27.1}_{-9.6}$	20.7	1.839(f); 1.853(i); 1.867 (r)
$2.33^{+0.05}_{-0.04}$	$1.65^{+0.76}_{-0.75}$	S I Kα	$45.7^{+21.1}_{-20.7}$	9.2	2.307

XMM–Newton was analysed and discussed by Grandi et al. (2004). The observed X-ray flux [F(0.2–10 keV) ∼3 × 10^{-13} erg cm^{-2} s^{-1} with 80 per cent emitted below 2 keV] was found to be comparable in the soft X-ray band to the emission of 3C 445 and could thus, in principle, strongly affect the *Suzaku* spectrum.

We note however that a contemporaneous *Swift* observation (of about 10 ks) of 3C 445 did not detect 1WGA J2223.7−0206 in the FOV of the *Swift*-XRT, suggesting that 1WGA J2223.7−0206 was much fainter during the *Suzaku* observation. We estimated an upper limit on its soft X-ray flux of ∼2 × 10^{-14} erg cm^{-2} s^{-1}. We also note that the observed soft X-ray fluxes of 3C 445 measured with *Chandra* and *Suzaku* are similar: F(0.5–2) keV ∼ 1.9 × 10^{-13} erg cm^{-2} s^{-1} and F(0.5–2) keV ∼ 2.3 × 10^{-13} erg cm^{-2} s^{-1} for the *Chandra* and *Suzaku* observations, respectively. This suggests that the X-ray emission of 1WGA J2223.7−0206 was not comparable to 3C 445, indeed the roll angle of the *Chandra* observation of 3C 445 was specifically set in order to avoid the contamination from narrow-line QSO.

As a last check, we searched also the *Chandra* source catalogue (Evans et al. 2010) and the *Chandra* XAssist source list (Ptak & Griffiths 2003) for X-ray bright sources within the XIS extraction radius. Three sources are detected with a 0.3–8 keV flux greater than 9 × 10^{-15} erg cm^{-2} s^{-1} and 1WGA J2223.7−0206 is the brightest among them with a 0.5–8 keV flux of about 5 × 10^{-14} erg cm^{-2} s^{-1}. Thus we inspected the *Chandra* ACIS-S spectrum of 1WGA J2223.7−0206, which has ∼300 net counts. In order to derive an estimate of the soft X-ray flux, we fitted the *Chandra* data with a single absorbed power-law component (Γ ∼ 1.7; $N_{\rm H}$ ∼ 3 × 10^{21} cm^{-2}). We found that also during the *Chandra* observation, 1WGA J2223.7−0206 was fainter than during the *XMM–Newton* pointing and its 0.5–2 keV observed flux was 1.6 × 10^{-14} erg cm^{-2} s^{-1}. We thus conclude that the contamination of this second AGN is minimal.

3.3 Modelling the Fe Kα line and the high-energy emission

We then considered the hard X-ray emission of 3C 445 using for the soft X-ray emission a single photoionized plasma plus a Gaussian emission line at ∼2.33 keV as described above and keeping the ionization parameter fixed to the best-fitting value. For the remainder of the analysis, we used again the XIS data grouped with a minimum of 100 count bin^{-1}. We examined simultaneously the *Suzaku* XIS (0.4–10 keV) and HXD-PIN data (15–65 keV) and the *Swift*-BAT, setting the cross-normalization factor between the HXD and the XIS-FI spectra to 1.16, and allowing the cross-normalization with the *Swift* data to vary, since the two observations are not simultaneous.

As shown in Fig. 2, the residuals at the energy of the Fe K band clearly reveal the presence of a strong narrow core at the expected energy of the Fe Kα line (6.4 keV), while no clear residuals are present at the energy of the Fe Kβ line. To model the Fe Kα line, we first added a narrow Gaussian line at the energies of Fe Kα; the inclusion of the line in the model improves the fit by $\Delta\chi^2 = 101$ for 3 degrees of freedom (χ^2/d.o.f. = 456.3/405). The Fe Kα core has an equivalent width of EW = 100 ± 14 eV with respect to the observed continuum, it is centred at $E = 6.383 \pm 0.012$ keV and has a measured width of $\sigma = 34 \pm 30$ eV. As suggested by the residuals, a Fe Kβ is not statistically required, however we found that the upper limit on its flux is 13.6 per cent of the Fe Kα line flux, consistent with the theoretical value. The amount of reflection ($R = 0.9 \pm 0.4$) is found to be consistent with the observed EW of the Fe Kα line, for an inclination angle $i = 60^\circ$ and Γ ∼ 1.8.

Finally, we note that in the XIS-FI data, there are still some line-like residuals redwards of the Fe Kα line. Upon adding a second narrow Gaussian line the fit only marginally improves (χ^2/d.o.f. = 445.1/403 corresponding to $\Delta\chi^2 = 11$ for 2 d.o.f.), significant at 99.6 per cent confidence from the F-test. If this emission line is real, the closest candidate for this feature could be the Compton shoulder to the Fe Kα line. We note however that its energy ($E = 6.05 \pm 0.11$ keV) is slightly lower than the expected value of the first scattering peak (E ∼ 6.24 keV). An alternative possibility is that this line is a redwing of a possible relativistic disc line. Thus we replaced the Gaussian with relativistic disc-line component (DISKLINE in XSPEC; Fabian et al. 1989); this code models a line profile from an accretion disc around a Schwarzschild black hole. The main parameters of this model are the inner and outer radii of the emitting region on the disc, and its inclination. The disc radial emissivity is assumed to be a power law, in the form of r^{-q}. For the fit we

fixed the emissivity $q = 3$ and the angle to 60°. The fit statistic is similar to the Gaussian profile (χ^2/d.o.f. = 446.6/402), and we found that the best-fitting parameters of this disc line correspond to emission from an annulus at $\sim 100 R_g$ (with $R_g = GM/c^2$) and with an EW = 75 ± 40 eV. The energy of this putative line, although not well constrained, is consistent with the ionized Fe line ($E = 6.64 \pm 0.16$ keV). Given the lower statistical significance and the uncertainties on the energy centroid of this possible emission line, we will not discuss it any further.

We then replaced the PEXRAV and Gaussian components with a more updated model for the Compton reflection off an optically thick photoionized slab of gas, which includes the Fe K emission line (REFLIONX; Ross & Fabian 2005; Ross, Fabian & Young 1999). We assumed solar abundances, and we found the fit is equally good (χ^2/d.o.f. = 453.8/405). As expected, the ionization of the reflector is found to be low, $\log\xi < 1.74$ erg cm s^{-1}, in agreement with the measured energy centroid of the Fe Kα emission line being close to the value for neutral iron (or less ionized than Fe XVII). We thus fixed the ionization parameter to $\xi = 10$ erg cm s^{-1}, which is the lower boundary for the REFLIONX model. We note that the residuals at ∼6.05 keV are still present; we thus keep in the model the additional redshifted emission line. The parameters of the absorber are consistent with the values obtained with the PEXRAV model ($N_{H1} = 1.0^{+0.1}_{-0.2} \times 10^{23}$ cm^{-2}and $N_{H2} = 3.2^{+0.3}_{-0.3} \times 10^{23}$ cm^{-2}, $f_{cov} = 0.78^{+0.02}_{-0.01}$). The photon index is now $\Gamma = 1.74^{+0.06}_{-0.05}$.

3.4 The X-ray absorber

Assuming that the absorber is neutral, the broad-band X-ray emission of 3C 445 requires the presence of two absorbers: one fully covering and one only partial covering. The best-fitting parameters of this model, which we now consider our best-fitting neutral absorber model, are listed in Table 3. This dual absorber plus reflection model is a good phenomenological description of the broad-band X-ray emission of 3C 445 ; however it may be too simple an approximation of a more complex absorber. We note also that, taking into account the optical classification of 3C 445 as type 1 AGN, the X-ray absorber is not likely to be a neutral absorber covering a large fraction of the nuclear source as derived with the above model. A possibility is that the absorber is mildly ionized and thus it is partially transparent and not efficient in absorbing the optical and soft X-ray emission.

To test this scenario, we then replaced both the partial and the fully covering neutral absorbers with a photoionized absorber, the latter is made using a multiplicative grid of absorption model generated with the XSTAR code (Kallman et al. 2004). For simplicity, we modelled the possible relativistic emission line with an additive Gaussian component, and we allowed to vary the Galactic absorption [$N_H = (0.63^{+0.22}_{-0.23}) \times 10^{21}$ cm^{-2}]. At first we assumed a zero outflow velocity of the absorber and we tested a single zone of absorption. The absorber is found to be mildly ionized ($\log\xi = 1.10^{+0.10}_{-0.24}$ erg cm s^{-1}) and with a column density similar to the neutral absorber $N_H = (1.89^{+0.09}_{-0.06}) \times 10^{23}$ cm^{-2}. We note also that the fit marginally improves with respect to the neutral absorber (χ^2/d.o.f. = 443.1/406) and overall the model is able to reproduce the curvature of the spectrum. The best-fitting parameters of this model are listed in Table 4.

A similar ionized absorber was also found with the *Chandra* observation ($\log\xi \sim 1.4$ erg cm s^{-1}, $N_H \sim 1.85 \times 10^{23}$ cm^{-2}); however, the LETG spectrum of 3C 445 suggested that this absorber is outflowing with a $v_{out} \sim 0.034c$, indeed this solution was statistically preferred to a zero outflow velocity ($\Delta C = 22$; Reeves et al. 2010). Thus we allowed the absorber to be outflowing, but this does not statistically improve the fit ($\Delta\chi^2 = 2$). The parameters of this absorber (N_H and $\log\xi$) are found to be similar to the case with no net velocity shift and albeit it is not well constrained the outflowing velocity is found to be slightly lower than the *Chandra* one ($v_{out} < 0.01c$).

To further investigate the apparent discrepancy between the *Chandra* and *Suzaku*'s results, we performed a joint fit of the two observations. Though the source is not highly variable, we allow the relative normalizations of the primary continuum and the parameters of the ionized absorber to vary. With this test we found that the intrinsic emission is slightly brighter during the *Suzaku* observation (∼10 per cent). As seen with the independent fit the N_H and $\log\xi$ of the ionized absorbers are found to be consistent within the two

Table 3. Summary of the neutral partial covering absorber model. The ionization parameters of the soft X-ray plasma is fixed to $\log\xi = 1.97$ erg cm s^{-1}. Fluxes are corrected only for Galactic absorption, while the luminosities are corrected for rest frame absorption.

Model Component	Parameter	Value
Power law	Γ	$1.74^{+0.06}_{-0.05}$
	Normalization	$3.82^{+0.63}_{-0.48} \times 10^{-3}$
Scattered component	Normalization	$9.9^{+0.5}_{-0.5} \times 10^{-5}$
Absorber	N_{H1}	$1.0^{+0.1}_{-0.2} \times 10^{23}$ cm^{-2}
Absorber	N_{H2}	$3.2^{+0.3}_{-0.3} \times 10^{23}$ cm^{-2}
	f_{cov}	$0.78^{+0.02}_{-0.01}$
Ionized reflection	ξ	10^a erg cm s^{-1}
	Normalization	$1.20^{+0.12}_{-0.13} \times 10^{-5}$
Ionized emission	Normalization	$2.2^{+0.6}_{-0.6} \times 10^{-6}$
	χ^2/d.o.f.	454/406
	$F_{(0.5-2)\,keV}$	2.71×10^{-13} erg cm^{-2} s^{-1}
	$F_{(2-10)\,keV}$	7.01×10^{-12} erg cm^{-2} s^{-1}
	$L_{(0.5-2)\,keV}$	7.1×10^{43} erg s^{-1}
	$L_{(2-10)\,keV}$	1.2×10^{44} erg s^{-1}
	$L_{(14-150)\,keV}$	3×10^{44} erg s^{-1}

[a]The ionization of the reflector has been fixed to the minimum value allowed by the model; if left free to vary the upper limit is found to be 55 erg cm s^{-1}.

Table 4. Summary of the ionized absorber model. Fluxes are corrected only for Galactic absorption, while the luminosity are corrected for rest frame absorption. The ionization of the emitter has been fixed to best fit value.

Model component	Parameter	Value
Power law	Γ	$1.85^{+0.05}_{-0.04}$
	Normalization	$4.79^{+0.42}_{-0.69} \times 10^{-3}$
Scattered component	Normalization	$10.2^{+0.6}_{-0.6} \times 10^{-5}$
Absorber	N_H	$1.89^{+0.09}_{-0.06} \times 10^{23}$ cm^{-2}
	$\log\xi$	$1.10^{+0.10}_{-0.24}$ erg cm s^{-1}
Ionized reflection	ξ	10^a erg cm s^{-1}
	Normalization	$1.26^{+0.15}_{-0.14} \times 10^{-5}$
Ionized emission	Normalization	$2.4^{+0.8}_{-0.7} \times 10^{-6}$
	χ^2/d.o.f.	443/406
	$F_{(0.5-2)\,keV}$	2.86×10^{-13} erg cm^{-2} s^{-1}
	$F_{(2-10)\,keV}$	7.03×10^{-12} erg cm^{-2} s^{-1}
	$L_{(0.5-2)\,keV}$	8.5×10^{43} erg s^{-1}
	$L_{(2-10)\,keV}$	1.3×10^{44} erg s^{-1}
	$L_{(14-150)\,keV}$	3×10^{44} erg s^{-1}

[a]The ionization of the reflector has been fixed to the minimum value allowed by the model.

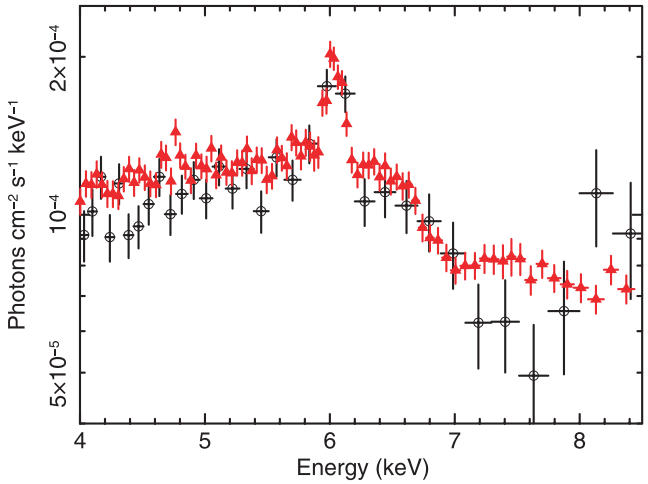

Figure 4. *Chandra* (black circles in the electronic version) and *Suzaku* XIS-FI (red triangles in the electronic version) spectra in the 4–8.5 keV band folded against a simple power-law continuum with the normalizations free to vary. In the high-energy part, the spectra show a sharper absorption feature in *Chandra* spectrum compared to a more shallow and possibly broader drop in the *Suzaku* data.

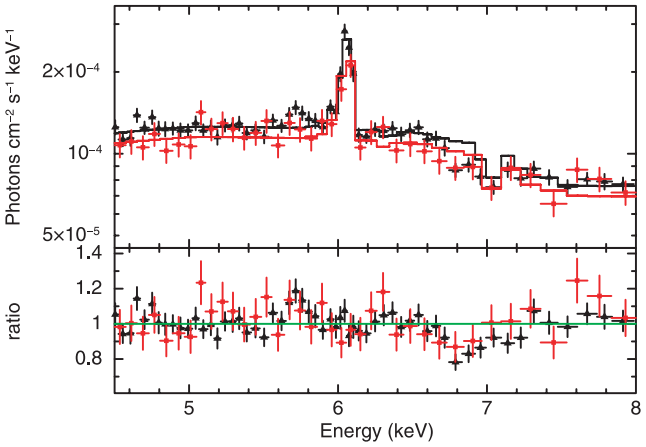

Figure 5. Upper panel: *Suzaku* XIS-FI (filled triangles, black in the electronic version), *XMM–Newton* EPIC-pn (filled squares, red in the electronic version) band folded against a single mildly ionized absorber model with the outflowing velocity fixed to the *Chandra* best-fitting value. Lower panel: data/model ratio to the above single ionized absorber. The XIS-FI and EPIC-pn residuals are consistent with each other. They both show a deficit of counts around ∼6.8 keV (observed frame, corresponding to ∼7.2 keV in the rest frame).

observations ($\Gamma \sim 1.73^{+0.22}_{-0.19}$, $N_{\rm H} \sim 1.85^{+0.09}_{-0.11} \times 10^{23}$ cm^{-2}, log$\xi \sim 1.4^{+0.20}_{-0.12}$ erg cm s^{-1}and $\Gamma \sim 1.85^{+0.05}_{-0.04}$, $N_{\rm H} \sim 1.89^{+0.09}_{-0.06} \times 10^{23}$ cm^{-2}, log$\xi \sim 1.1^{+0.10}_{-0.24}$ erg cm s^{-1}from the *Chandra* and *Suzaku* best fits, respectively; see also table 3 of Reeves et al. 2010) but not the outflowing velocities. The comparison between the *Chandra* and *Suzaku* data is shown in Fig. 4; in the *Suzaku* data the drop at high energies appears to be broader and less deep. We note that there is also a possible hint of a higher curvature of the *Chandra* spectrum, indeed the *Chandra* spectrum is below the *Suzaku* data, also between 4–6 keV. This could be a signature of a variation of the X-ray absorber, being less transparent during the *Chandra* observation. As we show below, with the present data and taking into account the complexity of the model we cannot confirm or rule out a modest variability of the absorber.

As a final check, we inspected the previous *XMM–Newton* observation, indeed also in that observation there was a hint of a possible absorption feature at 6.9 keV (Sambruna et al. 2007), though the underlying continuum shape was slightly different. In particular, lacking the high energy data, the amount of reflection could not be constrained. Taking into account that the source did not strongly vary (in shape and flux) between the two observations, we then simultaneously fitted the *XMM–Newton* and *Suzaku* spectra allowing the cross-normalization to vary and we tested a single ionized absorber (with no outflowing velocity). We found that the *XMM–Newton* spectrum is remarkably in agreement with the *Suzaku* one. In particular, we note that the residuals are similar also redwards of the Fe Kα emission line. However the short net exposure time of the *XMM–Newton* observation (∼15 ks) prevents us from further investigating the presence of a possible redwing of a relativistic Fe Kα line.

Two possible scenarios could explain the observed differences between the *Suzaku* and the *Chandra* observations, the first is that the absorber has indeed varied, with a lower ionization and outflowing velocity during the *Suzaku* pointing. A second possibility is that the broader drop seen in *Suzaku* is due to the presence of a more complex and possibly multiphase absorber. In order to test the second scenario, we fixed the outflowing velocity of the ionized absorber to the one seen with the *Chandra* observation. The fit is statistically worse ($\chi^2 = 496.7/406$ corresponding to a $\Delta\chi^2 = 53$) and clear residuals are present, both in the *XMM–Newton* and *Suzaku* spectra, at ∼7.2 keV (∼6.8 keV in the observed frame), which are reminiscent of a possible absorption feature. Indeed, the *Chandra* absorption feature appears to be slightly narrower and more blueshifted, compared to the drop in the *Suzaku* data. Forcing the low ionization absorber fitted to the *Suzaku* data to have the same outflow velocity as inferred from the *Chandra* observation results in a deficit of counts around 7 keV (observed frame) in the *Suzaku* and *XMM–Newton* spectra, when compared to the *Chandra* model (see Fig. 5).

The deficit could then be modelled with an additional absorption line in the *Suzaku* data, perhaps arising from a higher ionization absorber. As a first test, using only the *Suzaku* data, we included in the model an additional inverted Gaussian, statistically the fit is similar with respect to the single ionized absorber with no outflow velocity (χ^2/d.o.f. = 450.9/403). The energy of this line is found to be $E = 7.30 \pm 0.05$ keV (6.9 keV in the observed frame) and the EW $= 62^{+23}_{-22}$ eV, which would imply a column density of the absorber of about $N_{\rm H} \sim 10^{23}$ cm^{-2}. The closest candidate for this absorption feature is the $1 \rightarrow 2$ transition of Fe XXVI ($E = 6.97$ keV) blueshifted by $v \sim 0.05c$, while if the absorption is associated with lower ionization 1s–2p of Fe XXV ($E = 6.7$ keV), the corresponding blueshift will be higher ($v \sim 0.09c$).

We then tested a more complex model for the absorber including a second ionized absorber and leaving free to vary the outflow velocity of this absorber, while the outflow velocity of the mildly ionized absorber was fixed to best-fitting value found with *Chandra* ($v = 0.034c$). As for the mildly ionized absorber, we used a grid created with XSTAR, for this grid we assumed again solar abundances, a $\Gamma \sim 2$ illuminating continuum and, taking into account the apparent broadening of the absorption feature, we assumed a turbulent velocity of 3000 km s^{-1}. The addition of this second absorber does not statistically improve the fit with respect to the scenario with a single ionized absorber with no net velocity shift (χ^2/d.o.f. = 453/403). This absorber if found to be fast outflowing $v \sim 0.04c$ highly ionized log $\xi > 4.7$ erg cm s^{-1}and high column density

$N_{\rm H} \sim 10^{24}\,{\rm cm}^{-2}$($N_{\rm H} = 2.8^{+0.8}_{-2.6} \times 10^{24}\,{\rm cm}^{-2}$). It is important to note that the significance of this second absorber is hindered by the choice of the underlying continuum model and more importantly by the choice of outflow velocity of the mildly ionized absorber.

The simplest interpretation is that there is a modest variability of the mildly ionized absorber, while we cannot rule out the presence of a second highly ionized absorber. To distinguish between these scenarios we need higher spectral resolution observations, such as the one that will be provided with the *ASTRO-H* calorimeter.

4 DISCUSSION AND CONCLUSIONS

To summarize, the *Suzaku* data confirm the complexity of the X-ray emission of 3C 445. The soft X-ray spectrum is dominated by several emission lines, which require the presence of at least one ionized emitter with $\log\xi \sim 1.97\,{\rm erg\,cm\,s^{-1}}$ and which is in agreement with the results obtained with our deep *Chandra* observation. The primary X-ray continuum is strongly obscured by an absorber with a column density of $N_{\rm H} = 2{-}3 \times 10^{23}\,{\rm cm}^{-2}$, which could be either a neutral partial covering absorber or a mildly ionized absorber. Independently from the model assumed for the absorber, the broad-band *Suzaku* spectrum allowed us to detect a relatively strong reflection component.

Overall, the X-ray spectrum of 3C 445 is remarkably similar to a type 2 Seyfert galaxy, which could be at odds with its classification as a type 1 AGN. The main characteristics resembling a type 2 Seyfert galaxy are the presence of soft X-ray emission lines as well as the presence of a high column density X-ray absorber. As we will discuss in the next sections, two competitive scenarios could explain the X-ray emission of 3C 445, both requiring that our line of sight is not completely blocked towards the central engine since we have evidence that we can see the emission from the BLRs (Eracleous & Halpern 1994). We will show that our deep *Suzaku* observation combined with a recent *Chandra* observation, with the high-resolution grating LETG, strongly suggest that both the absorption and the soft X-ray lines originate within the putative torus, and we are not seeing the source through a uniform and cold absorber.

4.1 The soft X-ray emission, similarity and differences to type 2 Seyfert galaxies

The *Suzaku* spectrum confirms the presence of several soft X-ray emission lines, as previously detected with the *XMM–Newton* observation, from oxygen, neon, magnesium and silicon. In particular, we detected a line at ∼0.88 keV, which if associated with the O VIII RRC would strongly implies emission from a photoionized plasma as seen in Compton-thin Seyfert galaxies (Bianchi et al. 2006; Guainazzi & Bianchi 2007). As already shown with the *XMM–Newton* observation, a physical model for the observed soft X-ray emission requires the presence of one or two ionized emitters, with ionization levels within the range of obscured RQ-AGN (Guainazzi & Bianchi 2007).

The limited spectral resolution of the XIS data does not allow us to resolve the lines, thus using only the *Suzaku* data we cannot measure the density of this plasma and place strong constraints on the location of the emitter. However, as 3C 445 is rather constant in flux, we could use the results obtained with the long *Chandra* LETG observation, indeed assuming the same abundances we found that the soft X-ray emission can be similarly described with two ionized emitters with the same ionization ($\log \xi_1 \sim 1.95\,{\rm erg\,cm\,s^{-1}}$ and $\log \xi_2 \sim 3.17\,{\rm erg\,cm\,s^{-1}}$) and luminosity as during the *Chandra* observation. The *Chandra* data provided also the first measurement of the densities ($n_e > 10^{10}\,{\rm cm}^{-3}$) and distance ($R \sim 0.01$–$0.1$ pc; Reeves et al. 2010) of these soft X-ray emitters, which are suggestive of a location within the putative torus and reminiscent of the BLR. Furthermore, in the *Chandra* data several lines were resolved into their forbidden and intercombination line components, and the velocity widths of the O VII and O VIII emission lines were determined ($v_{\rm FWHM} \sim 2600\,{\rm km\,s^{-1}}$). Assuming Keplerian motion, this line broadening implies an origin of the gas on subparsec scales (Reeves et al. 2010). 3C 445 is not an isolated example, indeed there are other well-known cases of type 1 Seyfert galaxies where the soft X-ray emission lines appear to be produced in the BLR (e.g. MKN 841, Longinotti et al. 2010; Mrk 335, Longinotti et al. 2008, NGC4051, Ogle et al. 2004; NGC 5548, Steenbrugge et al. 2005).

Thus the emerging scenario is that the soft X-ray emission 3C 445 is not produced in a region coincident with the optical narrow-line region, as in obscured RQ Seyfert galaxies. A possible origin of these lines in the BLR is also in agreement with the multiwavelength properties of 3C 445, indeed the optical classification as a type 1 AGN, suggests that our line of sight towards the BLR is not completely blocked by a high column density absorber. This photoionized emitter also resembles the 'warm gas' observed in more than 50 per cent RQ Seyferts 1 (Crenshaw et al. 2003), which acts as a 'warm mirror' and at the same time intercepts the line of sight producing absorption features. As we will discuss below these photoionized clouds that we are seeing in emission might be associated with the absorber responsible for the curvature of the X-ray continuum.

4.2 The X-ray absorber/reflector: a distant reflector?

The *Suzaku* spectrum, and in particular the data above 10 keV, allows us to confirm the presence of a strong reflection component and for the first time to provide a measurement of its intensity. The presence of this component was already suggested with the *BeppoSAX* observation (Grandi et al. 2006; Dadina 2007), indeed 3C 445 was detected with the PDS instrument. However, taking into account the large FOV of this detector and the presence of a nearby ($z = 0.09$) and bright cluster A2440 (located only 30 arcmin away), it was not possible to derive strong constraints on the amount of reflection. The presence of a strong reflection component was also suggested by the intensity of the Fe Kα line detected in the *BeppoSAX* and in the *XMM–Newton* observations (EW ∼ 120 eV Sambruna et al. 2007), which was consistent with being produced in reflection off a medium with high column density (Turner et al. 1997; Murphy & Yaqoob 2009).

Thanks to the smaller FOV of the HXD and more importantly to the *Swift*-BAT detection we can now confirm the presence of this component. In particular, both the positional accuracy (∼2 arcmin) and offset with respect to 3C 445 (∼0.5 arcmin) reported in 54-months Palermo-BAT catalogue (Cusumano et al. 2010) are compatible with the emission from the centre of 3C 445. As shown in Fig. 6, the averaged *Swift*-BAT spectrum is in agreement with the one obtained with *Suzaku*. This suggests that there is no strong variability of the intrinsic emission, but more importantly that contamination from the nearby cluster is unlikely to be present.

As shown in Section 3.3, the amount of reflection measured is $R \sim 0.9$ implying a covering factor of the cold reflector of about 2π sr. Furthermore, as we showed in the previous section the primary X-ray emission of 3C 445 is obscured by a high column density absorber ($N_{\rm H} \sim 10^{23}\,{\rm cm}^{-2}$) with a covering factor of about

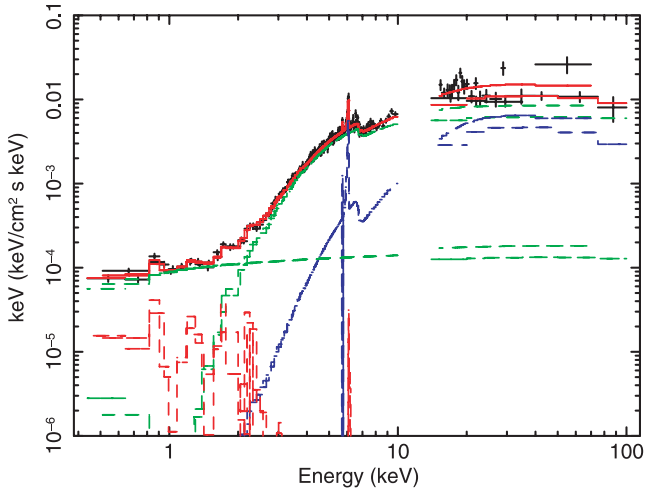

Figure 6. *Suzaku* and *Swift*-BAT spectra (black data points) of 3C 445. Data have been rebinned for plotting purposes. The AGN continuum model is composed of a primary power-law component transmitted trough an ionized absorber and a scattered power-law component. The narrow Fe Kα line and the reflection component are modelled with the REFLIONX model. The possible relativistic component is modelled with a single-redshifted Gaussian line. The soft X-ray emission lines are accounted for with an ionized emitter.

80 per cent. In the hypothesis that the absorber is neutral the predicted extinction in the optical band would then far exceed the observed reddening of the source [$E(B-V) \sim 1$; Crenshaw et al. 1988]. In particular, a scenario where our line of sight intercepts a homogeneous parsec-scale torus is difficult to reconcile with the observational evidence, from the soft X-ray and optical band, that we are seeing the innermost region of this AGN. On the other hand, the inclination angle from the jet ($\sim$60°) combined with the current estimates of the average opening angle of the 'torus' implies that we might be looking at the nucleus of 3C 445 on the edge of this putative torus.

Though we note that the data with a high-resolution calorimeter at the Fe Kα line energy are necessary to resolve the line complex and provide more stringent constraints on the linewidth, the measured Fe Kα width FWHM $< 7000\,\mathrm{km\,s^{-1}}$ is consistent with the width of the soft X-ray lines measured with the *Chandra* LETG data (Reeves et al. 2010) and with the measured FWHM of the Hα ($\sim$6400 $\mathrm{km\,s^{-1}}$; Eracleous & Halpern 1994) and Hβ ($\sim$3000 $\mathrm{km\,s^{-1}}$). The Fe Kα line could then be in part produced either in the outer part of the accretion disc or in the BLR. We note however that the relatively high EW of the Fe Kα line implies the presence of a Compton thick reflector, which is also confirmed by the detection of a strong reflection component. Indeed in order to be produced in transmission the observed EW of Fe Kα requires a higher column density absorber than the one measured with lower energy cut-off.

We thus tested the new model for the toroidal reprocessor[6] (Murphy & Yaqoob 2009), keeping the soft X-ray emitter modelled with a single ionized zone, and we found that the intensity of the Fe Kα line and of the higher energy emission require the presence of a reprocessor with a column density $N_{\rm H} \sim 6.5 \times 10^{23}\,\mathrm{cm^{-2}}$ viewed at $\sim$60°, which is remarkably in agreement with the inclination of the system as derived from the radio observations (Eracleous & Halpern 1998). We note however that the photon index is now harder ($\Gamma \sim 1.5$) and there are some residuals in the 2–5 keV band, suggesting the presence of a second absorber. We thus included a second and ionized absorber with no net outflowing velocity, qualitatively we note that we now have an excellent representation of the overall curvature of the X-ray emission. While the parameters of the ionized absorber are similar to the one derived with the REFLIONX model, we found that the reprocessor responsible for the Fe Kα line has a column density of $N_{\rm H} \sim 1.4 \times 10^{24}\,\mathrm{cm^{-2}}$ and as before it is viewed at $\sim$60°, the photon index is now $\Gamma \sim 1.8$. Qualitatively both these tests show us that a high column density mirror responsible for the Fe Kα line and the Compton reflection component is present and it could be associated with the part of the putative torus lying close to the plane of the accretion disc.

One possibility is that the photoionized emission line clouds, although located closer to the central SMBH, are lifted above the system's equatorial plane; our line of sight would then intercept the high column density absorber/reflector on a subparsec scale but also have an unobscured view of BLR emission, where the optical and soft X-ray emission lines are produced. The alternative scenario which is suggested by the clumpy and neutral absorber, required to model the X-ray emission of 3C 445, is that the absorber/reflector is not a uniform 'donut-like' structure and as proposed in recent models (Risaliti, Elvis & Nicastro 2002; Elitzur 2008; Maiolino et al. 2010) is clumpy and composed by many small and dense clouds, which could extend further in with respect to putative torus and are not simply obscuring the BLR but are part of the BLR themselves (Risaliti et al. 2009a,b). In this hypothesis our line of sight could then intercept a rather large number of clouds, which absorb/reflect the primary continuum but at the same time may also produce the broad emission lines from innermost ionized clouds.

4.3 The nature of the X-ray absorber: a variable ionized absorber?

As shown in Section 3.4, an alternative scenario to a clumpy and neutral absorber is an ionized absorber. This scenario naturally accounts for the discrepancy between the optical and the X-ray band, indeed this mildly ionized absorber could be similar to the warm absorbers observed in the X-ray spectra of RQ-AGN (Crenshaw, Kraemer & George 2003; Blustin et al. 2005; McKernan, Yaqoob & Reynolds 2007; Turner & Miller 2009), which appear to be outflowing with velocity of 100–1000 $\mathrm{km\,s^{-1}}$ and could be associated with the presence of disc winds (King & Pounds 2003).

As discussed in a companion paper (Reeves et al. 2010) the presence of an ionized absorber, with the same ionization level and column density, associated with a disc wind is strongly supported by the deep observation with high spectral resolution which provides more stringent constraints on the velocity of this absorber ($v_{\rm out} = 0.034 \pm 0.002c$) and on the launch radius ($R \sim 10^{16}$–10^{17} cm). As also shown in that paper, at this distance the likely density of the absorbing gas would be $\sim 10^{10}\,\mathrm{cm^{-3}}$, which would imply a $\Delta R \sim 10^{13}$ cm and a $\Delta R/R \sim 10^{-3}$ and thus suggesting a highly clumped absorber. It was also suggested that the clumpiness of this absorber would produce short-time-scale variations of the observed column density, as seen in other Seyferts.

Indeed, the observed difference between the *Chandra* and *Suzaku* spectra could be explained with variability of this low ionization absorber, not in terms of the covering factor or $N_{\rm H}$ of the absorber but in terms of its velocity. This is not surprising indeed not only redshifted and blueshifted absorption lines are predicted in several theoretical models of failed disc winds (Proga & Kallman 2004; Sim et al. 2010) or of aborted jet (Ghisellini, Haardt & Matt 2004),

[6] http://www.mytorus.com/

but also these models predict the outflows to be unstable and to show variability. In particular, outflows and jets could be produced intermittently and/or they could not have enough power to escape the system and eventually fall back into the accretion disc. This will affect the expected signatures that this warm gas imprints on the primary X-ray emission, which will produce transient absorption features and variability of the derived outflowing velocities and their EW as observed in several sources (Dadina et al. 2005; Risaliti et al. 2005; Braito et al. 2007; Porquet et al. 2007; Turner et al. 2008; Miller et al. 2010; Turner et al. 2010; Lobban et al. 2011).

An alternative scenario ascribes the difference between *Chandra* and *Suzaku* spectra to a further ionized and fast outflowing absorption component, detected only with the *Suzaku* observation and characterized by a high ionization and column density ($N_{\rm H} \sim 10^{24}\,{\rm cm}^{-2}$). In this scenario the properties of the low ionization absorber are thus the same as the one derived with the *Chandra* observation (i.e., distance $R \sim 10^{16}$–10^{17} cm and clumpiness $\Delta R/R \sim 10^{-3}$). For the high ionization absorber, although in the *Suzaku* data the parameters of this absorber not well constrained, we can derive an order of magnitude estimate on its likely location from the values measured for the ionization parameter ($\xi \sim 5\,{\rm erg\,cm\,s}^{-1}$), the outflow velocity ($v_{\rm out} \sim 0.04c$) and the column density. We can thus use the relation between these quantities and the illuminating continuum luminosity: $L_{\rm ion}/\xi = nR^2$, where $L_{\rm ion}$ is the intrinsic 1–1000 Rydberg luminosity ($3 \times 10^{44}\,{\rm erg\,s}^{-1}$), assuming the thickness of the clouds $\Delta R = N_{\rm H}/n$ is less than the distance R, $\Delta R/R \ll 1$ we found $R < 5 \times 10^{15}$ cm (or $\sim$0.001 pc), which points towards an association of this absorbers with a wind launched off the disc at a subparsec distance from the central BH.

We note that both these ionized absorber scenarios imply that we are seeing a clumpy and possibly variable absorber located close to the central X-ray source. This could be associated with the presence of a disc wind which either is launched sporadically or it is highly clumped. However, in the absence of any stringent constraints on the launch radius, we cannot speculate more as to whether these two absorbers are part of a single clumpy wind, where the lower ionization component is associated to higher density clouds confined in the homogeneous highly ionized flow, or if the two components are part of single stratified medium. In order to determine whether it is a single and variable ionized absorber or a multiphase wind would require higher resolution observations with instruments such as the calorimeter which will fly with *ASTRO-H*. These observations will allow to establish the complex nature and kinematics of this absorber confirming the presence of blueshifted absorption lines from highly ionized iron.

5 CONCLUSION

We have presented the results of a deep *Suzaku* observation of the BLRG 3C 445 which shows a complex absorbed X-ray spectrum. We confirm the results obtained with the previous *XMM–Newton* observation which unveiled the presence of several soft X-ray emission lines. The *Suzaku* and *Swift* spectra allowed us to measure a strong reflection component, which we associate with the presence of a high column density matter which is not in the line of sight. The primary X-ray continuum is strongly absorbed either by a partially covering neutral or a mildly ionized absorber, which could be associated with an accretion disc wind.

Regarding the overall geometry of 3C 445, we know from the radio observations that we are seeing the central regions of this AGN at a relatively large inclination. A plausible scenario is that we are viewing along the edge of the putative torus through either a partially covering neutral absorber or mildly ionized absorber, which could be associated with an equatorial disc wind. In both the scenarios with an ionized or neutral absorber, the matter needs to be clumped, such as that the observer has a direct view of the clouds responsible of the soft X-ray and optical lines, which could be in part uplifted with respect to the equatorial plane. A possible schematic diagram for the geometry of the inner regions of 3C 445 is presented in fig. 8 of Reeves et al. (2010), a new addition to that schematic view is that *Suzaku* provided evidence for the presence also of a Compton-thick reflector. We find no evidence that our line of sight intercepts this Compton-thick absorber which is responsible for the reflected component and Fe Kα line. This absorber could be either associated with denser clouds probably located in the equatorial plane of the torus or of the clumpy absorber or the outer part of the disc wind.

ACKNOWLEDGMENTS

This research has made use of data obtained from the *Suzaku* satellite and data obtained from the High Energy Astrophysics Science Archive Research Center (HEASARC), provided by NASA's Goddard Space Flight Center. VB acknowledges support from the UK STFC research council.

REFERENCES

Antonucci R., 1993, ARA&A, 31, 473
Ballantyne D. R., 2007, Modern Phys. Lett. A, 22, 2397
Ballantyne D. R., Fabian A. C., Ross R. R., 2002, MNRAS, 329, L67
Baumgartner W. H. et al., 2010, ApJS, submitted
Bianchi S., Guainazzi M., Chiaberge M., 2006, A&A, 448, 499
Blustin A. J., Page M. J., Fuerst S. V., Branduardi-Raymont G., Ashton C. E., 2005, A&A, 431, 111
Boldt E., 1987, Phys. Rep., 146, 215
Braito V. et al., 2007, ApJ, 670, 978
Brinkman A. C. et al., 2000, ApJ, 530, L111
Cattaneo A. et al., 2009, Nat, 460, 213
Crenshaw D. M., Peterson B. M., Wagner R. M., 1988, AJ, 96, 1208
Crenshaw D. M., Kraemer S. B., George I. M., 2003, ARA&A, 41, 117
Cusumano G. et al., 2010, A&A, 510, A48
Dadina M., 2007, A&A, 461, 1209
Dadina M., Cappi M., Malaguti G., Ponti G., de Rosa A., 2005, A&A, 442, 461
Dickey J. M., Lockman F. J., 1990, ARA&A, 28, 215
Elitzur M., 2008, New Astron. Rev., 52, 274
Elvis M., 2006, Mem. Soc. Astron. Ital., 77, 573
Eracleous M., Halpern J. P., 1994, ApJS, 90, 1
Eracleous M., Halpern J. P., 1998, ApJ, 505, 577
Evans I. N. et al., 2010, ApJS, 189, 37
Fabian A. C., 2010, in Peterson B., Somerville R. S., Storehl-Bergmann T., eds, Proc. IAU Symp 267, Co-evolution of Central Black Holes and Galaxies. Kluwer, Dordrecht, p. 341
Fabian A. C., Rees M. J., Stella L., White N. E., 1989, MNRAS, 238, 729
Ghisellini G., Haardt F., Matt G., 2004, A&A, 413, 535
Grandi P., Foschini L., Masetti N., Palazzi E., 2004, A&A, 418, 907
Grandi P., Malaguti G., Fiocchi M., 2006, ApJ, 642, 113
Grandi P., Guainazzi M., Cappi M., Ponti G., 2007, MNRAS, 381, L21
Gruber D. E., Matteson J. L., Peterson L. E., Jung G. V., 1999, ApJ, 520, 124
Guainazzi M., Bianchi S., 2007, MNRAS, 374, 1290
Kallman T. R., Palmeri P., Bautista M. A., Mendoza C., Krolik J. H., 2004, ApJS, 155, 675
King A. R., Pounds K. A., 2003, MNRAS, 345, 657
Kokubun M. et al., 2007, PASJ, 59, 53
Koyama K. et al., 2007, PASJ, 59, 23

Kronberg P. P., Wielebinski R., Graham D. A., 1986, A&A, 169, 63
Leahy J. P., Black A. R. S., Dennett-Thorpe J., Hardcastle M. J., Komissarov S., Perley R. A., Riley J. M., Scheuer P. A. G., 1997, MNRAS, 291, 20
Liedahl D. A., 1999, in Van Paradijs J., Bleeker J. A. M., eds, Lecture Notes Phys. Vol. 520, X-ray Spectroscopy in Astrophysics. Springer, Berlin, p. 189
Lobban A. P., Reeves J. N., Miller L., Turner T. J., Braito V., Kraemer S. B., Crenshaw D. M., 2011, preprint (arXiv:1102.1894)
Longinotti A. L., Nucita A., Santos-Lleo M., Guainazzi M., 2008, A&A, 484, 311
Longinotti A. L. et al., 2010, A&A, 510, A92
McKernan B., Yaqoob T., Reynolds C. S., 2007, MNRAS, 379, 1359
Magdziarz P., Zdziarski A. A., 1995, MNRAS, 273, 837
Maiolino R. et al., 2010, A&A, 517, A47
Miller L., Turner T. J., Reeves J. N., Lobban A., Kraemer S. B., Crenshaw D. M., 2010, MNRAS, 403, 196
Mitsuda K. et al., 2007, PASJ, 59, 1
Murphy K. D., Yaqoob T., 2009, MNRAS, 397, 1549
Murphy E. M., Lockman F. J., Laor A., Elvis M., 1996, ApJS, 105, 369
Narayan R., Yi I., 1995, ApJ, 444, 231
Ogle P. M., Mason K. O., Page M. J., Salvi N. J., Cordova F. A., McHardy I. M., Priedhorsky W. C., 2004, ApJ, 606, 151
Porquet D. et al., 2007, A&A, 473, 67
Proga D., Kallman T. R., 2004, ApJ, 616, 688
Ptak A., Griffiths R., 2003, in Payne H. E., Jedrzejewski R. I., Hook R. N., eds, ASP Conf. Ser. Vol. 295, Astronomical Data Analysis Software and Systems XII. Astron. Soc. Pac., San Francisco, p. 465
Reeves J. N., Turner M. J. L., 2000, MNRAS, 316, 234
Reeves J. N., Sambruna R. M., Braito V., Eracleous M., 2009, ApJ, 702, L187
Reeves J. N., Gofford J., Braito V., Sambruna R., 2010, ApJ, 725, 8
Risaliti G., Elvis M., Nicastro F., 2002, ApJ, 571, 234
Risaliti G., Bianchi S., Matt G., Baldi A., Elvis M., Fabbiano G., Zezas A., 2005, ApJ, 630, L129
Risaliti G. et al., 2009a, MNRAS, 393, L1
Risaliti G. et al., 2009b, ApJ, 696, 160
Ross R. R., Fabian A. C., 2005, MNRAS, 358, 211
Ross R. R., Fabian A. C., Young A. J., 1999, MNRAS, 306, 461
Rudy R. J., Tokunaga A. T., 1982, ApJ, 256, L1
Sambruna R. M., Eracleous M., Mushotzky R. F., 1999, ApJ, 526, 60
Sambruna R. M., Eracleous M., Mushotzky R. F., 2002, New Astron. Rev., 46, 215
Sambruna R. M., Reeves J. N., Braito V., 2007, ApJ, 665, 1030 (SO7)
Sambruna R. M. et al., 2009, ApJ, 700, 1473
Sim S. A., Proga D., Miller L., Long K. S., Turner T. J., 2010, MNRAS, 408, 1396
Spergel D. N. et al., 2003, ApJS, 148, 175
Steenbrugge K. C. et al., 2005, A&A, 434, 569
Takahashi T. et al., 2007, PASJ, 59, 35
Tombesi F., Sambruna R. M., Reeves J. N., Braito V., Ballo L., Gofford J., Cappi M., Mushotzky R. F., 2010, ApJ, 719, 700
Torresi E., Grandi P., Guainazzi M., Palumbo G. G. C., Ponti G., Bianchi S., 2009, A&A, 498, 61
Torresi E., Grandi P., Longinotti A. L., Guainazzi M., Palumbo G. G. C., Tombesi F., Nucita A., 2010, MNRAS, 401, L10
Tueller J. et al., 2010, ApJS, 186, 378
Turner T. J., Miller L., 2009, A&AR, 17, 47
Turner T. J., George I. M., Nandra K., Mushotzky R. F., 1997, ApJ, 488, 164
Turner T. J., Reeves J. N., Kraemer S. B., Miller L., 2008, A&A, 483, 161
Turner T. J., Miller L., Reeves J. N., Lobban A., Braito V., Kraemer S. B., Crenshaw D. M., 2010, ApJ, 712, 209

This paper has been typeset from a TEX/LATEX file prepared by the author.